EXPERIMENTAL AND COMPARATIVE STUDY OF OPTICAL PROPERTIES OF DIFFERENT PHANTOMS BY THE KUBELKA–MUNK FUNCTION APPROACH **

Hüseyin Okan Durmuş [1,2*], Baki Karaböce [2], MirHasan Yu Seyidov [1]

[1] Department of Physics, Gebze Technical University, Kocaeli, Turkey; e-mail: hokandurmus@gtu.edu.tr
[2] Medical Metrology Laboratory, TUBITAK National Metrology Institute (TUBITAK UME), Kocaeli, Turkey

We optically characterized agar, muscle, and Zerdine phantoms mimicking human tissues. To the best of our knowledge, optical parameters for agar, muscle, and Zerdine phantoms have not been optimally determined in the literature. For this reason, this novel study makes significant contributions to the literature and there is an important innovation and originality in the optical characterization of these materials. With this research based on the phantoms, in this article we make important contributions to possible future studies, including optical device design and imaging technique development, system validation studies, etc. In other words, characterization studies on materials that imitate tissue in light-tissue interactions can provide important information to researchers and practitioners. In optical characterization, basic parameters such as the absorption coefficient, reduced scattering coefficient, and anisotropy factor, are evaluated as distinguishing characteristics, and these are referred to as microscopic optical properties in the literature. In this study, the optical properties of the aforementioned three different phantoms were experimentally investigated and compared with each other's. First, the macroscopic optical properties of the phantoms, including the absorbance, transmittance, reflectance, refractive index, and attenuation coefficient, were measured using a single integrated sphere and a spectrometer equipped with a broadband white light source within the wavelength range 200 to 1000 nm. Then, using the Kubelka–Munk function method, microscopic optical properties, which are the absorption coefficient, scattering coefficient, and reduced scattering coefficient, were determined based on the data of these macroscopic properties.

Keywords: *agar, Zerdine, and muscle phantom, microscopic and macroscopic optical properties, spectrometer, single integrating sphere, broadband white light source.*

ИССЛЕДОВАНИЕ ОПТИЧЕСКИХ СВОЙСТВ РАЗЛИЧНЫХ ФАНТОМОВ С ПОМОЩЬЮ ФУНКЦИИ КУБЕЛКИ–МУНКА

H. O. Durmuş [1,2*], B. Karaböce [2], M. Y. Seyidov [1]

УДК 543.42

[1] Технический университет Гебзе, Коджаэли, Турция; e-mail: hokandurmus@gtu.edu.tr
[2] Национальный институт метрологии TUBITAK (TUBITAK UME), Коджаэли, Турция

(Поступила 9 февраля 2022)

Исследованы оптические свойства трех различных фантомов из агара, мышц и Zerdine — материалов, имитирующих ткань. С использованием одной интегрированной сферы и спектрометра, оснащенного широкополосным источником белого света в диапазоне длин волн 200—1000 нм, измерены макроскопические оптические свойства фантомов: поглощение, пропускание, отражательная способность, показатель преломления и коэффициент затухания. С использованием функции Кубелки–Мунка на основе этих данных определены микроскопические оптические свойства — коэффициент поглощения, коэффициент рассеяния и приведенный коэффициент рассеяния.

Ключевые слова: *фантом, агар, Zerdine, мышца, микро- и макроскопические оптические свойства, спектрометр, одиночная интегрирующая сфера, широкополосный источник белого света.*

**Full text is published in JAS V. 90, No. 1 (http://springer.com/journal/10812) and in electronic version of ZhPS V. 90, No. 1 (http://www.elibrary.ru/title_about.asp?id=7318; sales@elibrary.ru).

Introduction. Light and optical techniques have had profound effects in modern medicine, and these effects continue today. Optical technologies are increasingly used in every field of medicine because of the non-invasive nature of the lights they use. Currently, there are a variety of applications for optical devices used in clinical practice to assess health and treat diseases. Light technologies are intensively used in all medical applications including diagnosis, surgery, and treatment. The following optical devices and applications can be given as examples in the diagnostic field: control of the external ear canal and eardrum with an otoscope; eye control with an ophthalmoscope and a retinoscope; a laryngoscope used in intubation; a head mirror used as a light-collecting and -focusing tool during a medical examination; pulse oximetry; endoscopy; colonoscopy; optical coherence tomography; spectroscopy; visualization of blood vessels and microcirculation; monitoring of blood oxygenation and tissue metabolism; imaging of skin cancer, drug tracking, micro-vessel and particle distribution; and photoacoustic imaging. Some examples of optical applications used in the field of surgery are also as follows: tissue laser ablation; tissue coagulation and cutting; refractive correction in the eye; dermatological laser treatments; removal of dental caries and cardiovascular plaques; and laser hair removal. Last, the following examples can be given of the light technologies and applications used in the field of treatment: blue light phototherapy, UV therapy, photodynamic therapy, low-level laser therapy, intense pulsed light therapy and LED therapy [1–3].

There are many publications in the literature on the optical properties of a wide variety of biological tissues, such as skin, brain, breast, bone, liver, kidney, lung, muscle, heart, blood, bowel, tumor, prostate, and fatty tissues [4–8]. It is difficult to measure the optical properties of biological tissues because they are turbid in terms of optical transparency. Accurate measurement of the optical properties of turbid media is vital for the development of biomedical diagnostic and therapeutic devices. Turbid media are described by fundamental optical properties, such as scattering and absorption components. For this, the light distribution in the turbid medium is modeled using parameters such as the absorption coefficient (μ_a), scattering coefficient (μ_s), anisotropy factor (g), and reduced scattering coefficient (μ_s') [9–11].

To measure the optical properties of tissues, there are two types of experimental techniques: direct and indirect. Direct methods rely solely on the experimental results. However, indirect (inverse) methods require a theoretical light-scattering model to be used in the experiment. In direct experimental methods, either the reflection emitted from the sample or the light transmittance passing through the sample is measured [10]. In the literature, tissues are characterized as in vitro using techniques such as the solution of the radiative transfer equation, integrating sphere spectroscopy, the Kubelka–Munk (KM) model, inverse adding-doubling, and inverse Monte Carlo simulation methods [1, 11–16].

Phantoms or tissue-mimicking materials (TMMs) have been widely used as test objects for many years in education, in imaging and therapeutic applications, and in medical research because they simulate properties that are highly similar to those of actual biological tissues. TMMs play a vital role in medical research as idealized tissue models for designing and testing methods, systems, and clinical tools [17, 18]. Phantoms, or tissue-mimicking materials, are materials that are used as reference test objects, particularly in preclinical testing, owing to their ability to simulate soft tissues and the advantages of being inexpensive and reusable. In the medical field, phantoms are used in fields such as device development, device performance evaluation, medical device testing, calibration, and clinical training. The fact that phantoms can be used repeatedly by imitating the properties of living tissues provides great advantages, particularly in medical research [19–28]. The phantoms are anticipated to be characterized and developed for their intended use. According to their intended use, phantoms can be characterized in various ways, including optical, thermal, mechanical, acoustic, and electrical properties. Although parameters such as sound velocity, characteristic acoustic impedance, and acoustic attenuation coefficient are examined in the acoustic characterization, optical parameters such as absorption coefficient, scattering coefficient, and anisotropy factor are measured in optical characterization. Phantoms should be created with the functions of the regions they will serve in mind. For instance, if they will be used in the ultrasonic field, their acoustic characterizations must be performed, and if they will be used in the optical field, their optical characterizations must be performed. Moreover, they must be manufactured according to the desired characteristics of the tissues and/or organs to be used [29, 30].

Phantoms are employed in the optical field for various purposes, including imaging technique development and image-guided interventions, system validation, optimization, stability evaluation, and medical device verification [31–33].

The KM model is a well-known theoretical reflectance model in optics. According to this model, some light passing through a homogeneous sample is scattered and absorbed in two directions, resulting in a reduction in light. The KM model is a two-flux approach to the theory of universal radiation transfer. The KM

scattering and absorption coefficients, denoted *S* and *K*, respectively, characterize the propagation of upward and downward fluxes. Radiation transfer models have frequently been employed to define the optical properties of light-scattering materials. One of the most successful and easy models is the KM model. This model, which employs the effective absorption and scattering coefficients of the material, can be used to calculate the optical properties of particulate films under diffused light. Examples of applications for the KM model in materials analysis include paints, decorative and protective coatings, pigmented plastics or polymers, solar-absorbing pigments and paints, human tissues, leaves, biological systems, crystalline materials, solids, powders, fibers and wool, papers, thermal insulation, and optical properties. In this method, the optical properties of the coating are represented by two constants: the absorption and scattering coefficients [34–37]. The key variables controlling light propagation in tissues are the absorption coefficient (μ_a), scattering coefficient (μ_s), and scattering anisotropy factor (g). Both the tissue structure (scattering) and chromophore concentration (absorption) determine the degree of these properties [38]. In optical characterization, three essential parameters are considered distinguishing characteristics: the absorption coefficient, the reduced scattering coefficient, and the anisotropy factor, which are known as microscopic optical qualities in the literature [39].

The purpose of this article is to provide more in-depth quantitative measurements of the optical properties of various tissue-mimicking phantoms and conduct an extensive investigation. In short, the optical properties of three distinct phantom materials, agar, Zerdine, and muscle phantom, were investigated and their results were compared in this study. First, the macroscopic optical properties of the phantoms, including absorbance, transmittance, reflectance, refractive index, and attenuation coefficient, were acquired using a single integrated sphere and a spectrometer equipped with a broadband white light source within the wavelength range 200 to 1000 nm. Then, using the KM function method, microscopic optical properties, which are the absorption coefficient, scattering coefficient, and reduced scattering coefficient, were determined based on the data of these macroscopic properties.

Methodology. Three distinct types of phantoms, agar, Zerdine, and muscle phantom were used. The agar phantom was prepared with 125 mL of distilled water, 6.8 g of $ZnCl_2$ and 2.5 g of agar [40]. The thickness of the agar phantom was 22 mm. The Zerdine® phantom was manufactured using the formulation described in Zerhouni and Rachedine's patent document. The thickness of the Zerdine phantom was 12 mm [41]. A muscle phantom identical to that published by Gutierrez et al. [42] was produced using 2.3 g of agar, 10.7 g of aluminum oxide and 125 mL of distilled water. The thickness of the muscle phantom was 20 mm.

Optical characterization setup. The optical equipment included a compact spectrometer (Thorlabs, CCS200/M) with a wavelength range from 200 to 1000 nm, a broadband stabilized fiber-coupled white light source (Thorlabs, SLS201L/M), and a single integrating sphere (Thorlabs IS200 type 2 integrating sphere). Computations were realized by using Thorlabs OSA software and MS Excel. After the light was sent to the measuring system, the continuous flow of data was recorded by pausing each measurement within 5 s. In addition, all optical measurement experiments were carried out under controlled laboratory ambient conditions (temperature was 23.5±0.2°C and relative humidity was 45.0±5.0%rh).

Assessment of the optical data. During the measurement, the spectrum of the incoming light was obtained first. The light spectrum was obtained in the absence of the phantom material in the experimental setup. To remove background noise in the dark environment, the same measurement was repeated by closing the light cover of the single integrating sphere. The primary signal was thus obtained by subtracting the signal of the dark environment from the "incoming light" signal obtained at the beginning. The phantom was then placed into the system and the spectrum of the phantom was recorded. The dark background noise was again eliminated to produce a real phantom signal. The I_0 data are represented by the main signal, whereas the I signal is represented by the real phantom signal. From the acquired Main Signal (Light–Dark) and Real Phantom (Phantom–Dark) data, macroscopic and microscopic optical properties were finally obtained.

Calculation of optical properties. Optical properties, such as absorbance, transmittance, reflectance, refractive index, and linear or total attenuation coefficient, were measured and calculated using equations:

$$R + T + A = 1 \text{ or } \%R + \%T + \%A = 100\% \text{ [43]}, \quad (1)$$

$$A = -\log(I/I_0) = -\log(T) = 2 - \log(\%T) \text{ [44]}, \quad (2)$$

$$T = I/I_0 \text{ [44]}, \quad (3)$$

$$R = 1 - (A + T) \text{ [43]}, \quad (4)$$

$$R = \frac{(n-1)^2}{(n+1)^2} \text{ [43]}, \quad (5)$$

$$I = I_0 e^{-\mu x},\ \mu = -\frac{\ln I/I_0}{x}\ [45], \tag{6}$$

where n is the refractive index; T is transmittance; R is reflectance; μ is the linear or total attenuation coefficient.

The KM function is characterized by [46]:

$$F(R) = \frac{(1-R)^2}{2R} = k/s, \tag{7}$$

where k is the absorption coefficient; s is the scattering coefficient.

The total attenuation coefficient is described by [47]:

$$\mu = \mu_t = \mu_a + \mu_s, \tag{8}$$

where μ_a is the absorption coefficient, and μ_s is the scattering coefficient. That, is $k = \mu_a$ and $s = \mu_s$ can be matched using Eqs. (7) and (8).

The reduced scattering coefficient (μ_s') is defined by the following equation [48]:

$$\mu_s' = (1-g)\mu_s, \tag{9}$$

where g is the anisotropy factor.

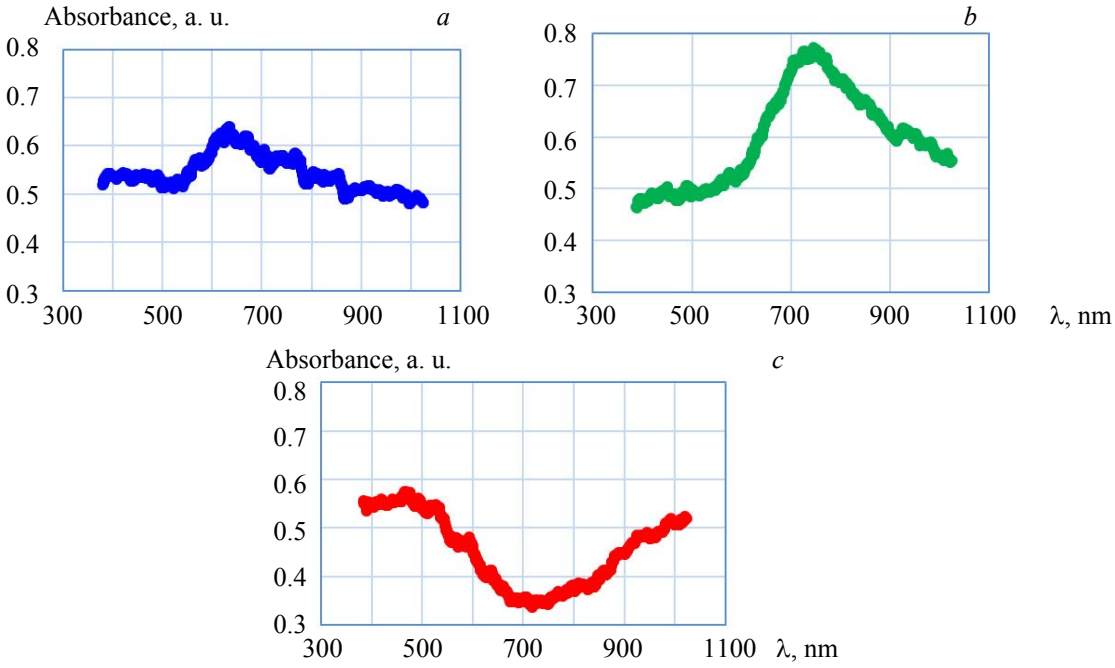

Fig. 1. The measured averaged curves of absorbance graphs of agar (a), muscle (b), and Zerdine (c) phantoms, respectively.

Results and discussion. The measurement results for the macroscopic and microscopic optical parameters are presented as follows. A minimum of six measurements were conducted while measuring the optical properties of phantoms. For example, the averaged curves of the absorbance graphs of all the studied phantoms are shown in Fig. 1. Because the experimental conditions did not change, a single averaged curve for the absorbance graph of phantoms was given. In these measurements, the individual maximum points were determined, and the average peak values were calculated for each phantom. Using the absorbance values at the peak values in each single measurement for each phantom, all other optical parameters were calculated for this peak value of each phantom by means of the given Eqs. (1)–(9). As a result, the mean and standard deviation values were calculated for each optical parameter in the six measurements obtained for each phantom, and the results are presented here.

The macroscopic optical characteristics of all the phantoms are shown in Figs. 2 and 3. Figure 2 shows the determined peak wavelengths, and absorbance, transmittance, and reflectance values of all phantoms at the peak wavelengths. Figure 3 shows the determined refractive indices and linear attenuation coefficient values of all phantoms at the peak wavelengths.

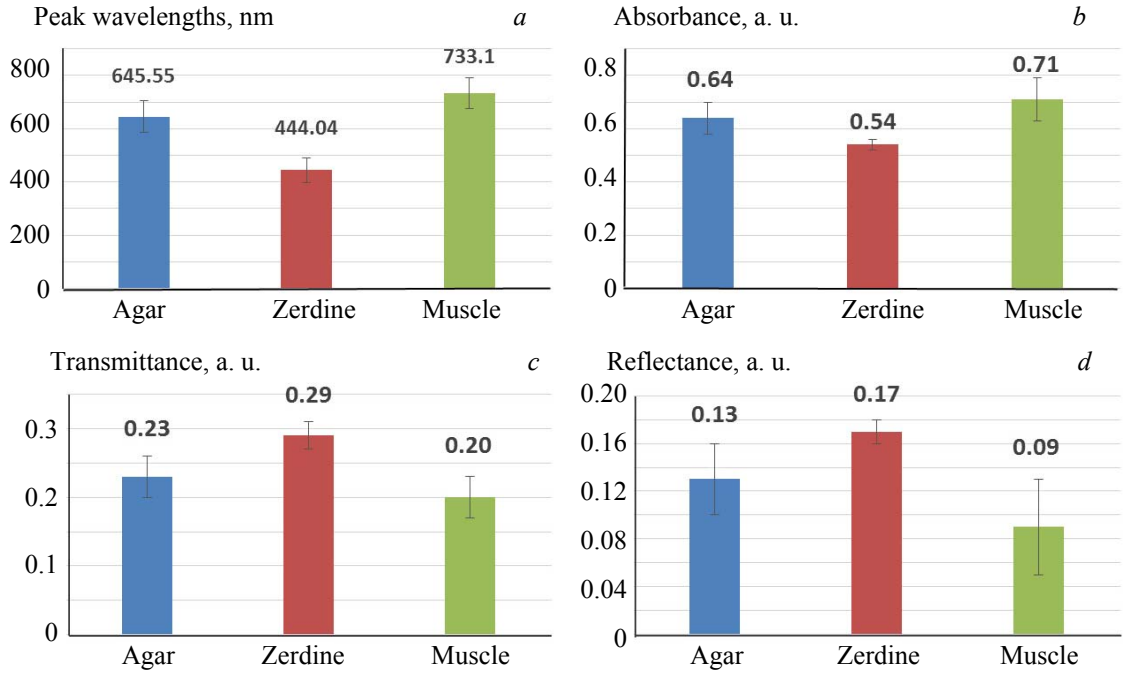

Fig. 2. The determined peak wavelengths of all the phantoms (a), and absorbance (b), transmittance (c), and reflectance (d) values determined at the peak wavelengths.

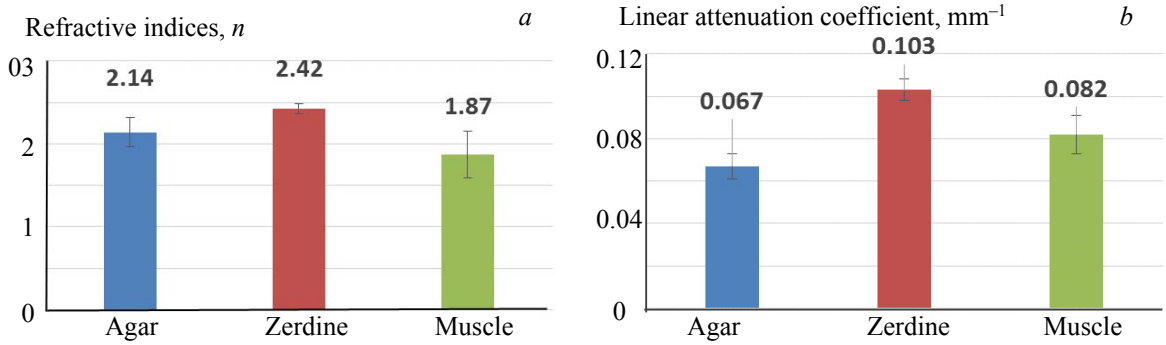

Fig. 3. The refractive indices (a) and linear attenuation coefficient (b) values of all the phantoms at the peak wavelengths.

By using these macroscopic optical properties, microscopic optical properties such as the absorption coefficient, scattering coefficient, and reduced scattering coefficient determined at the peak wavelengths were calculated with the help of the KM function approach. μ_t is calculated from Eq. (6) and the known R value (Eq. (4)) is the reflectance value. Then, Eqs. (7) and (8) are solved together, and μ_a and μ_s are found separately. Anisotropy factor value $g = 0.98$ for the muscle phantom and $g = 0.9$ for the agar and Zerdine phantoms have been used to find the reduced scattering coefficient in the calculations.

Figure 4 shows the typical determined microscopic optical characteristics of the phantoms, such as the absorption coefficient, scattering coefficient, and reduced scattering coefficient at peak wavelengths.

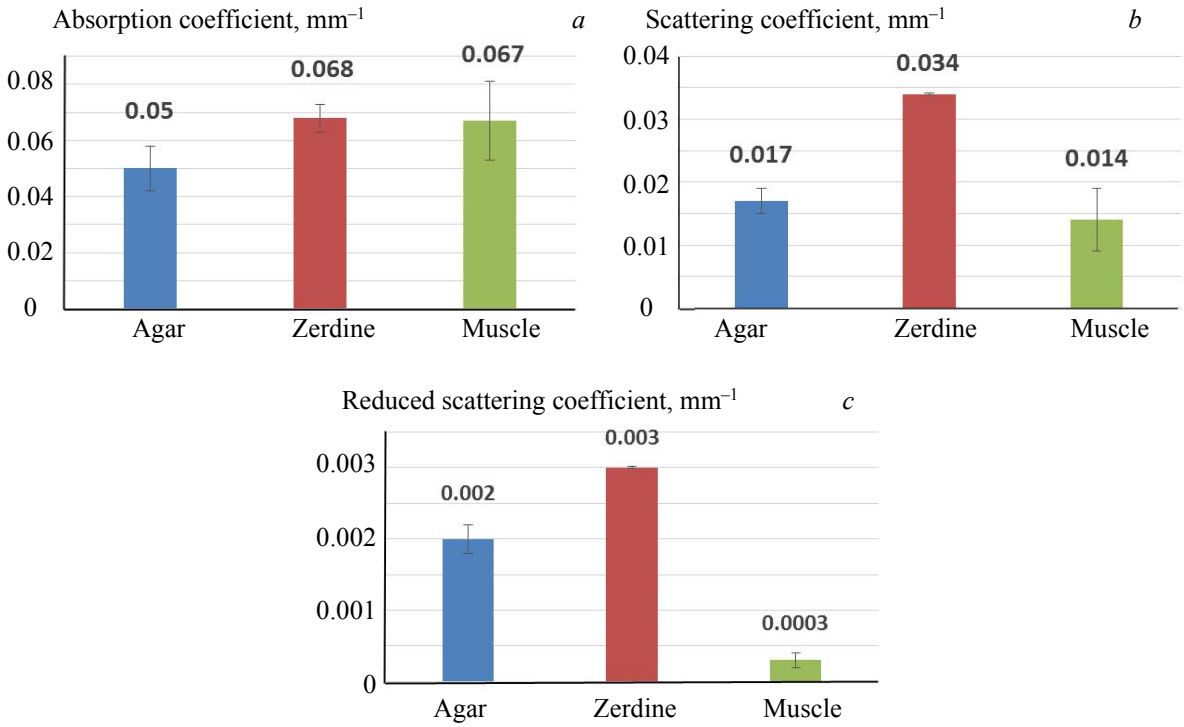

Fig. 4. The determined absorption coefficient (a), scattering coefficient (b), and reduced scattering coefficient (c) values of all the phantoms at the peak wavelengths.

The macroscopic and microscopic optical properties of agar, Zerdine, and muscle phantoms were investigated using a spectrometer with a single integrated sphere and a broadband white light source within the wavelength range 200—1000 nm. In fact, the spectra were originally obtained between 200 and 1000 nm. However, because the resolution of the signals was so high, so was the noise level. The moving average of the data was used to reduce the noise level and obtain smoother signals. For this reason, the spectrum range in the graphics was obtained between 400 and 1000 nm.

For optical characterization, the absorption coefficient was used as a reference, and the results were evaluated. Absorbance peak values for the agar phantom were determined within the range 645.55±61.05 nm and the absorption coefficient was found to be 0.050±0.008 mm^{-1}. This value is compatible with those reported in [49]. Again, the absorbance peak values found for the muscle phantom were within the range 733.10±57.33 nm and the absorption coefficient was found to be 0.067±0.014 mm^{-1}. This value is also in good agreement with the values reported in the literature. For example, the absorption coefficients found for muscle tissue (e.g., porcine muscle and bovine muscle) in an in vitro study on animal tissues ranged from 0.053 to 0.065 mm^{-1} [50]. For the Zerdine phantom, the absorbance peak values were within the range 444.04±46.96 nm and the absorption coefficient was found to be 0.068±0.005 mm^{-1}. However, no other study was found in the literature for the Zerdine phantom other than our group's study. For comparison, an evaluation can be made from the refractive index obtained in our previous publication [51]. The refractive index of the Zerdine phantom at 635 nm using the homogeneous medium measurement method in our previous study was found to be 1.99±0.41. This value corresponds to a refractive index of between 1.58 and 2.4. However, the refractive index found in the stated study is between 2.36 and 2.48, but the present study must be evaluated at wavelengths of 444.04±46.96 nm. Therefore, it can be said that there is a slight overlap in the refractive index values.

Conclusions. With the latest optical technologies developed, the optical properties of living tissues alone can provide sufficient information to identify diseases, especially cancer, or to monitor tissue metabolism. Recently, a variety of techniques for determining tissue optical properties have been developed. Visible and near-infrared wavelengths of light are frequently used in these techniques. It is well known how challenging it is to determine optical properties of tissues in vivo. Numerous errors have a major impact on the measurements. For this reason, studies performed on phantoms by isolating specific tissue types are general-

ly considered as a reliable technique in the field of research. For successful and safe applications in optics-related medical treatments, it is necessary to determine the optical properties of biological tissues, such as the absorption coefficient (μ_a), reduced scattering coefficient (μ_s'), scattering coefficient (μ_s), anisotropy factor (g), and refractive index (n). Therefore, it is crucial to optically characterize tissue-mimicking phantoms before using them under real conditions. In this study, macroscopic and microscopic optical properties of agar, Zerdine, and muscle phantoms were determined for the first time by the current research, using the Kubelka–Munk function approach method. This study allows the investigation of optical parameters based on different wavelengths. Our proposed approach investigates the values of the optical parameters along a spectrum rather than searching for optical parameters at a particular wavelength. That is why this study, which was carried out based on spectroscopy, makes the investigation of optical properties unique. As a result, optical characterization of phantoms can be easily performed using this method, and this method can be applied to many different types of phantoms in future studies.

REFERENCES

1. A. N. Bashkatov, K. V. Berezin, K. N. Dvoretskiy, M. L. Chernavina, E. A. Genina, V. D. Genin, V. V. Tuchin, *J. Biomed. Opt*., **23**, No. 9, 091416 (2018).
2. S. H. Yun, S. J. Kwok, *Nat. Biomed. Eng*., **1**, No. 1, 1–16 (2017).
3. https://link.springer.com/chapter/10.1007/978-3-319-31903-2_13
4. S. L. Jacques, *Phys. Med. Biol*., **58**, No. 11, R37 (2013).
5. V. K. Nagarajan, V. R. Gogineni, S. B. White, B. Yu, *Int. J. Hyperthermia*, **35**, No. 1, 176–182 (2018).
6. W. F. Cheong, S. A. Prahl, A. J. Welch, *IEEE J. Quantum Electron*., **26**, No. 12, 2166–2185 (1990).
7. A. N. Bashkatov, E. A. Genina, V. V. Tuchin, *J. Innovative Opt. Health Sci*., **4**, No. 1, 9–38 (2011).
8. M. J. van Gemert, R. Verdaasdonk, E. G. Stassen, G. A. Schets, G. H. Gijsbers, J. J. Bonnier, *Lasers Surg. and Med*., **5**, No. 3, 235–237 (1985).
9. F. Fanjul-Vélez, J. L. Arce-Diego, Proc. 21st Int. Conf. Radioelektronika 2011, 1–4 (2011).
10. M. R. Shenoy, B. P. Pal, *Appl. Opt*., **47**, No. 17, 3216–3220 (2008).
11. X. Liu, Y. Wu, *Solar Energy Mater. Solar Cells*, **223**, 110972 (2021).
12. D. Sardar, L. Levy, *Laser. Med. Sci*., **13**, 106–111 (1998).
13. D. K. Sardar, B. G. Yust, F. J. Barrera, L. C. Mimun, A. T. Tsin, *Laser. Med. Sci*., **24**, No. 6, 839–847 (2009).
14. A. Shahin, W. Bachir, M. S. El-Daher, *Polish J. Med. Phys. Eng*., **27**, No. 1, 99–107 (2021).
15. María M. Pérez, Ana Ionescu, Ana Yebra, Juan C. Cardona, Luis J. Herrera, María José Rivas, Óscar E. Pecho, Razvan Ghinea, *Proc. SPIE*, **10453** (2017), https://doi.org/10.1117/12.2276308.
16. E. Zamora-Rojas, B. Aernouts, A. Garrido-Varo, W. Saeys, D. Pérez-Marín, J. E. Guerrero-Ginel, *Innovative Food Sci. Emerging Technol*., **20**, 343–349 (2013).
17. C. K. McGarry, L. J. Grattan, A. M. Ivory, F. Leek, G. P. Liney, Y. Liu, C. H. Clark, *Phys. Med. Biol.* (**2020**).
18. G. Rajeshkumar, R. Vishnupriyan, S. Selvadeepak, Tissue Mimicking Material an Idealized Tissue Model for Clinical Applications: A Review Materials Today: Proceedings, **22**, 2696–2703 (2020), https://doi.org/10.1016/j.matpr.2020.03.4.
19. V. Cheruparambath, S. Sampath, L. N. Deshikar, H. M. Ismail, K. Bhuvana, *Indian J. Critic. Care Med.*, **16**, No. 3, 163 (2012).
20. M. O. Culjat, D. Goldenberg, P. Tewari, R. S. Singh, *Ultrasound Med. Biol*., **36**, No. 6, 861–873 (2010).
21. K. Wang, C. C. Ho, C. Zhang, B. Wang, *Engineering*, **3**, No. 5, 653–662 (2017).
22. O. Sieryi, A. Popov, V. Kalchenko, A. Bykov, I. Meglinski, *Proc. SPIE*, **11363** (2020), https://doi.org/10.1117/12.2560174.
23. S. Khan, S. Hollenbach, S. Goswami, F. Feng, S. A. McAleavey, *IEEE Int. Ultrasonics Symposium (IUS)*, 1–3 (2020); doi: 10.1109/IUS54386.2022.9958924.
24. J. R. Cook, R. R. Bouchard, S. Y. Emelianov, *Biomed. Opt. Express*, **2**, No. 11, 3193–3206 (2011).
25. R. Srinivasan, D. Kumar, M. Singh, *Trends Biomater. Artif. Organs*, **15**, No. 2, 42–47 (2002).
26. C. Kim, A. Garcia-Uribe, S. R. Kothapalli, L. V. Wang, *Proc. SPIE*, **6870** (2008), https://doi.org/10.1117/12.766773.
27. A. Bitarafan-Rajabi, H. Hasanzadeh, M. Jahangiri, Z. Hoseinpour, H. Nazemi, A. Baghian, H. Moladoust, *Arch. Cardiovascular Imaging*, **2**, No. 2 (2014).

28. B. W. Pogue, M. S. Patterson, *J. Biomed. Opt*., **11**, No. 4, 041102 (2006).
29. H. O. Durmus, F. Sametoglu, B. Karaboce, M. Y. Seyidov, "Investigation of Macroscopic and Microscopic Optical Properties of Agar-Based IEC Phantom", Middle East International Conference on Contemporary Scientific Studies-V, Ankara, 27–28/03/2021 (2021).
30. H. O. Durmus, E. Ari, B. Karaboce, M. Yu, *Results Optics*, **5**, 100142 (2021).
31. A. I. Chen, M. L. Balter, M. I. Chen, D. Gross, S. K. Alam, T. J. Maguire, M. L. Yarmush, *Med. Phys*., **43**, No. 6, 3117–3131 (2016).
32. P. Lai, X. Xu, L. V. Wang, *J. Biomed. Opt*., **19**, No. 3, 035002 (2014).
33. E. Dong, Z. Zhao, M. Wang, Y. Xie, S. Li, P. Shao, R. X. Xu, *J. Biomed. Opt*., **20**, No. 12, 121311 (2015).
34. *McGraw-Hill Dictionary of Scientific & Technical Terms*, 6th ed., McGraw-Hill Companies, Inc. (2003).
35. L. Yang, B. Kruse, *JOSA*, **21**, No. 10, 1933–1941 (2004).
36. W. E. Vargas, G. A. Niklasson, *Appl. Opt*., **36**, No. 22, 5580–5586 (1997).
37. A. B. Murphy, *J. Phys. D: Appl. Phys*., **39**, No. 16, 3571 (2006).
38. T. Lindbergh, M. Larsson, I. Fredriksson, T. Strömberg, *Proc. SPIE*, **6435**, 64350I (2007); https://doi.org/10.1117/12.698903.
39. C. J. Hourdakis, A. Perris, *Phys. Med. Biol*., **40**, No. 3, 351 (1995).
40. E. Çetin, H. O. Durmuş, B. Karaböce, N. Kavaklı, IEEE Int. Symposium Medical Measurements and Applications (MeMeA), 1–5 (2019), doi: 10.1109/MeMeA.2019.8802203.
41. M. B. Zerhouni, M. Rachedine, In: Ultrasonic Calibration Material and Method, Ed. Google Patents (1993).
42. M. I. Gutierrez, S. A. Lopez-Haro, A. Vera, L. Leija, *BioMed Res. Int.* (**2016**).
43. M. Y. Nadeem, W. Ahmed, *Turkish J. Phys*., **24**, No. 5, 651–659 (2000).
44. D. T. Harvey, *Analytical Chemistry for Technicians*, 3rd ed., John Kenkel (2003).
45. S. Chang, A. K. Bowden, *J. Biomed. Opt*., **24**, No. 9, 090901 (2019).
46. J. O. S. E. Torrent, V. Barrón, *Mineral. Methods*, **5**, 367–385 (2008).
47. B. C. Wilson, In: *Optical-Thermal Response of Laser-Irradiated Tissue*, Springer, Boston, MA, 233–303 (1995).
48. E. J. Jeong, H. W. Song, Y. J. Lee, S. J. Park, M. J. Yim, S. S. Lee, B. K. Kim, *BioChip J*., **11**, No. 1, 67–75 (2017).
49. L. Ntombela, B. Adeleye, N. Chetty, *Heliyon*, **6**, No. 3, e03602 (2020).
50. P. Sun, Y. Wang, *Opt. Laser Tech*., **42**, No. 1, 1–7 (2010).
51. H. O. Durmuş et al., *IEEE Int. Symposium on Medical Measurements and Applications (MeMeA)* (2020), doi: 10.1109/MeMeA49120.2020.9137206.